Spatiotemporal changes in along-tract profilometry of cerebellar peduncles in cerebellar mutism syndrome

Sebastian M Toescu[1,2,3,4*], Lisa Bruckert[1], Rashad Jabarkheel[5], Derek Yecies[5], Gerald Grant[5], Kristian Aquilina[4], Chris Clark[3], Kshitij Mankad[6], Heidi Feldman[1], Katie Travis[1], Kristen Yeom[1,2]

1. Division of Developmental-Behavioural Pediatrics, Stanford University School of Medicine, Stanford, CA 94305, USA
2. Department of Radiology, Lucille Packard Children's Hospital, Stanford University School of Medicine, Stanford, CA 94305, USA
3. Developmental Imaging and Biophysics Section, UCL-GOS Institute of Child Health, 30 Guilford St, London, WC1N 1EH, UK
4. Department of Neurosurgery, Great Ormond Street Hospital, London, WC1N 3JH, UK
5. Department of Neurosurgery, Lucille Packard Children's Hospital, Stanford University School of Medicine, Stanford, CA 94305, USA
6. Department of Radiology, Great Ormond Street Hospital, London, WC1N 3JH, UK

Author:

Sebastian M Toescu, Neurosurgery ST3, North Thames Deanery

SBNS Associate Member

s.m.toescu@gmail.com

Abstract

Cerebellar mutism syndrome occurs in 25% of children following resection of posterior fossa tumours. Characterised by mutism, emotional lability and cerebellar motor signs, the syndrome is usually reversible over weeks to months. Its pathophysiology remains unclear, but evidence from diffusion MRI studies has implicated damage to the superior cerebellar peduncles in the development of this condition. This essay describes the results of an automated tractography analysis of the cerebellar peduncles, providing a high-resolution spatiotemporal profile of diffusion MRI changes in cerebellar mutism syndrome.

Thirty children with medulloblastoma (mean age ± standard deviation 8.8 ± 3.8 years) underwent volumetric T1-weighted and diffusion MRI at four timepoints over one year. Forty-nine healthy children (9.0 ± 4.2 years), scanned at a single timepoint, were included as age- and sex-matched controls. CMS status was determined by contemporaneous casenote review. Automated Fibre Quantification (AFQ) was used to segment each subject's cerebellar peduncles, and fractional anisotropy was computed at 30 nodes along each tract. A non-parametric permutation-based method was used to generate a critical cluster size and p-value for by-node ANOVA group comparisons. Z-scores for patients' fractional anisotropy at each node were calculated based on values from controls' corresponding nodes; these were analysed using mixed ANOVA with *post-hoc* false discovery rate-corrected pairwise t-tests.

13 patients developed cerebellar mutism syndrome overall. Fractional anisotropy was significantly lower in the distal regions of the superior cerebellar peduncle pre-operatively (p=0.0137), although patients could not be distinguished pre-operatively with respect to cerebellar mutism syndrome status. Post-operative reductions in fractional anisotropy in children with cerebellar mutism syndrome were highly specific to the distal superior cerebellar peduncle, and were most pronounced at follow-up timepoints (p=0.006). These results build on previous work implicating damage to the superior cerebellar peduncle in cerebellar mutism syndrome, and by describing these specific changes in unprecedented spatiotemporal resolution, are likely to have direct relevance to neurosurgeons performing posterior fossa tumour resection in children.

Keywords

Cerebellar mutism syndrome; Dentato-rubro-thalamo-cortical tract; Diffusion MRI; Medulloblastoma; Tractography.

Abbreviations

AC, anterior commissure; AC-PC, anterior-posterior commissural plane; AFQ, automated fiber quantification; ANOVA, analysis of variance; CMS, cerebellar mutism syndrome; dMRI, diffusion MRI; DRTC, dentato-rubro-thalamo-cortical tract; DTI, diffusion tensor imaging; FA, fractional anisotropy; ICP, inferior cerebellar peduncle; LPCH, Lucile Packard Children's Hospital; MCP, middle cerebellar peduncle; MNI, Montreal Neurological Institute; ROI, region of interest; TBSS, tract-based spatial statistics.

Funding

This work was conducted and written by the applicant (SMT), who visited Stanford University in Spring 2020 funded by a UCL Bogue Fellowship. SMT is funded by Great Ormond Street Hospital Children's Charity (award no 174385) and is an Honorary Research Fellow of the Royal College of Surgeons of England.

Word count (Introduction to Conclusions, excluding Figures / Tables and Legends) 4880

Introduction

Medulloblastoma is the most common malignant brain tumour of childhood. Resective surgery has a key role in its treatment, but is complicated by the development of post-operative cerebellar mutism syndrome (CMS) in up to a quarter of cases[1]. CMS is characterized by a delayed onset of mutism, emotional lability and cerebellar motor deficits[2]. Recovery, by way of speech dysarthria, usually occurs after several weeks, yet children are often left with longer-term linguistic and cognitive deficits[3–5]. A pathophysiological mechanism for CMS has proved elusive thus far. Evidence has converged on the proximal dentato-rubro-thalamo-cortical tract (DRTC) as being centrally implicated[6]. Efferent fibres of the DRTC originate in the dentate nucleus, travel through the superior cerebellar peduncle (SCP), decussate in the midbrain and ascend via the red nucleus and thalamus before projecting to widespread areas of the cerebral cortex[7–9]. The SCP thus contains almost all of the efferent cerebellar fibres, and it seems likely that damage to the SCP caused either by tumour or surgery, is an aetiological factor in CMS[6]. The role of the middle (MCP) and inferior cerebellar peduncles (ICP) in CMS is less clear, although there is some evidence of delayed structural changes in the inferior olivary nucleus following CMS[10].

Diffusion MRI (dMRI) studies, in which voxel-wise principal diffusion directions can be inferred based on models applied to empirical data, have been instrumental in studying this group of patients. Such an approach can be leveraged in two ways: firstly, to study the underlying microstructure of the brain; and secondly, to estimate long-range connections between brain regions, a process known as tractography. The diffusion tensor is the canonical model applied to dMRI data, and yields biophysically relevant metrics such as fractional anisotropy (FA). Higher FA is seen in directionally oriented tissue microstructure, such as in white matter, due to constraints on free diffusion of water imposed by axonal structures. FA has been widely reported in many dMRI studies of children with posterior fossa tumours, and has been shown to be reduced in the SCP in children who develop CMS post-operatively compared to those who do not[11–14]. Similarly, disruptions to tractography reconstructions of the DRTC have been shown in CMS[15]. Both of these approaches, however, suffer from drawbacks. Microstructural metrics are often averaged either across whole-brain white matter (i.e. tract-based spatial statistics[16] as in Morris et al.[11]), in regions-of-interest (ROIs)[13,14] or across the entire length of a tract[17,18] leading to a loss of spatial information on regional variation in FA. Tractography applied in individual patients – though useful to delineate anatomy – is a qualitative tool which is difficult to truly quantify[19]. A synergistic approach is

along-tract profilometry[20–22], which enables the quantification of a chosen diffusion microstructure metric along the axis of the tract. One such toolbox, automated fibre quantification (AFQ)[21], has yielded insights into brain-behaviour correlations for supratentorial white matter tracts. An extension has been developed to enable automated along-tract analysis of the cerebellar peduncles[23,24], and the feasibility of its clinical application has been demonstrated[25].

The aim of this essay is to describe differences in DTI metrics in the cerebellar peduncles between children with CMS, those without post-operative CMS, and healthy age- and sex-matched controls. This is achieved by segmenting the cerebellar peduncles longitudinally using AFQ, in a cohort of paediatric patients that underwent resective surgery of posterior fossa medulloblastomas. This will enable reporting of differences along the length of the cerebellar peduncles in high spatial resolution; and at high temporal resolution by sampling multiple time points before and after surgery.

Methods

Participants

A prospectively maintained neuro-oncology database of paediatric brain tumour patients treated at Lucile Packard Children's Hospital from 2002-2018 was retrospectively interrogated to extract clinical and demographic information on children with posterior fossa medulloblastoma. Contemporaneous clinical notes on these patients were reviewed to identify those who developed post-operative CMS. Patients were classified as having CMS if they showed the core symptom of mutism or reduced speech output in the early post-operative phase. Those without explicit mention of either normal speech or speech deficit in the post-operative clinical notes were classified as having indeterminate CMS status (n=4).

Imaging data were accessed for all patients, and scans were reviewed for the first post-operative year. Scans were grouped into four timepoints: pre-operative, immediate post-operative (< 7 days of tumour resection); early follow-up (1-4 months); and late follow-up (> 9 months). Patients with dMRI acquisition for at least one timepoint were included in the study. Supplementary Figure 1 shows dMRI availability in the entire cohort of eligible patients. Scans acquired between 4 and 9 months post-operatively were not included so as to increase the distinction between the follow-up timepoints. Twenty patients had more than one scan within a single timepoint. For all time points, the scan which was technically superior (i.e.

no movement artefact or missing sequences) was selected. When both scans were comparable in quality, the scan closest to the operation date for time points 1-3 or the scan closest to the 12-month post-op date for time point 4 was chosen.

Timepoint-specific age- and sex-matched healthy controls were selected from a cohort of 113 children and adolescents who presented at Lucile Packard Children's Hospital from 2010-2017. In all cases, had normal structural MRI scans and no known systemic conditions affecting the brain, or psychiatric or developmental disorders. Participant selection and results of along-tract cerebellar profilometry of this cohort of healthy children are detailed elsewhere[24]. If two control candidates had the same age, both were included in the comparison group in order to enrich the control dataset; if a control candidate had an identical age to a patient, but different sex, the subject was included; sex-matching was performed at a group level, ensuring balance in sexes.

MRI acquisition

MRI scans were acquired on a 3T GE MR750 Discovery (GE Healthcare, Waukesha, WI, USA) using an 8-channel head coil. Children aged up to 6 years old were sedated under general anaesthesia; some children aged 6–8 years were sedated based on individual maturity level and ability to tolerate the MRI exam. Both high-resolution T1-weighted (3D SPGR, TR = 7.76 ms, TE = 3.47 ms, FOV = 240 × 240 mm^2, acquisition matrix = 512 × 512, voxel size = 0.4688 × 0.4688 × 1 mm^3, orientation = axial) and diffusion-weighted images were acquired as part of the paediatric brain MRI protocol. Diffusion data were collected with a twice-refocused GRAPPA DT-EPI sequence (TR = 4000–6000 ms depending on slice coverage, TE = 76.59 ms, FOV = 240 × 240 mm^2, acquisition matrix = 256 × 256, voxel size = 0.9375 × 0.9375 × 3 mm^3) using a b-value of 1000 s/mm^2 sampling along 25 isotropically distributed diffusion directions. One additional volume was acquired at b = 0 at the beginning of each scan.

Image preprocessing

After file conversion from Dicom to NIFTI using *dcm2niix*[26], dMRI data were preprocessed using the open-source software mrDiffusion (github.com/vistalab/vistasoft/mrdiffusion) implemented in Matlab R2017b (Mathworks, Natick, MA, USA). The b0 image was registered to the patient's anatomical T1-weighted image, which had been centred on the anterior commissure (AC) and aligned to the AC-PC plane. The combined transform that resulted from motion correction and alignment to the T1-weighted image was

applied to the raw data (as well as the diffusion gradient tables), and the transformed images were resampled to 2 × 2 × 2mm isotropic voxels. The diffusion tensor was fitted using a 'least squares' method, and colour FA maps were co-registered to the T1-weighted image to visually confirm alignment.

White matter tract identification

The open-source toolbox Automated Fibre Quantification (AFQ)[21] implemented in Matlab R2017b was used to perform tractography for each subject in an automated fashion. AFQ first performs whole-brain tractography, then segments fibre tracts based on atlas ROIs warped into subject space; these fibre tracts are then refined and clipped to the ROIs before quantification of diffusion metrics at a user-defined number of locations, or 'nodes', along the tract. A detailed description of cerebellar AFQ methodology is provided by Bruckert *et al.*[24]. Briefly, deterministic whole-brain tractography using a streamlines tracking technique[27–29] was seeded from a white matter mask defined as voxels with an FA value greater than 0.15; tracking was terminated in voxels with an FA below 0.1. Fibres shorter than 20mm and longer than 250mm were discarded from the whole-brain tractogram. Non-linear registrations were used to warp ROIs from MNI space into subject space. The inferior cerebellar peduncles (ICP), superior cerebellar peduncles (SCP) and middle cerebellar peduncle (MCP) were segmented if fibres from the whole-brain tractogram passed through the relevant ROIs. The core of the tract is defined by 30 nodes along the tract and computing the robust mean position of the corresponding sample points. The robust mean was computed by estimating the three-dimensional Gaussian covariance of the sample points and removing fibres that were either more than 4 standard deviations away from the mean position of the tract or that differed more than 1 standard deviation in length from the mean length of the tract. Fibre tracts were then clipped to begin and end at the ROIs from which they were created.

Fibre renderings of each subject's tracts, at each timepoint, were visually inspected; those which did not conform to known anatomical configurations of cerebellar peduncles were discarded. None of the controls' fibre groups were discarded as these had previously been through a rigorous quality control process[24]. For each tract in each subject, FA was summarized at 30 equidistant nodes by taking a weighted average of all streamlines at that node.

Statistical Analysis

Results were imported into R (v3.6.1; R Core Team, 2017) for further analysis and graphics were created using the ggplot2[30], rstatix[31] and ggpubr[32] packages. For the along-tract profilometry analyses, one-way ANOVA tests were computed on a node-by-node basis for each cerebellar peduncle and timepoint, generating a p-value at each node (p_{var}). A nonparametric permutation-based method[33] was used to control for the 30 comparisons along the tract. This procedure produced a family-wise error corrected cluster size and a critical p-value (p_{min}) for each of the candidate tracts. Differences in nodal FA values were considered significant if two criteria were satisfied: 1) $p_{var} < p_{min}$; 2) criterion (1) satisfied in a sufficient number of adjacent nodes to meet the criteria for a family-wise error corrected cluster size (i.e. if cluster size = 8; ≥8 adjacent nodes required $p_{var} < p_{min}$).

To investigate group differences between children with CMS and those without, each subject's FA values were converted to Z-scores based on the age- and sex-matched controls' summary scores at each node, for corresponding timepoints and tracts. Each tract was then segmented into thirds. The proximal third in the SCPs corresponded to nodes closest to the dentate nucleus, and the distal third corresponded to nodes closest to the midbrain. The ICP nodes closest to the inferior olivary nucleus corresponded to the proximal third, and those in the cerebellum were the distal third. MCP nodes ascended from left to right along the extent of the tract. For each cerebellar peduncle and timepoint, patients' Z-scores were compared using a two-way mixed ANOVA, with a between-subjects factor of group (CMS vs no CMS), and a within-subjects factor of tract segment (1st third, 2nd third, 3rd third). For this segment of the analysis, a pre-specified α of 0.05 was chosen. *Post-hoc* false-discovery rate adjusted[34] pairwise t-tests were used to compare significant interactions between CMS status and tract segments.

Results

Thirty patients were included in this study, along with a total of 49 age- and sex-matched healthy controls. Twenty-one patients (70%) had dMRI scans available at multiple timepoints. Twenty-eight patients (93.3%) had midline tumours of the vermis or fourth ventricle; two patients had tumours in the cerebellar hemispheres. Table 1 shows the demographic information of the included patients and their age- and sex-matched controls at each timepoint. 26 patients in the cohort had known CMS status; CMS was present in 13 of these children. The proportion of children with CMS at each timepoint varied from 46.2-61.1%. At one year follow-up,

symptoms of CMS had resolved in 9/13 (69.2%). The remaining four children had ongoing speech pathology.

Table 1 | Demographics of included study participants.

		Scan timing (months post-op)	n	Age (y, mean±S.D.)*	CMS	CMS %	Male %
Pre-op	Patients	0	13	7.68 ± 3.31	6**	46.2	69.2
	Controls	N/A	25	7.79 ± 4.04	N/A	N/A	68.0
Post-op	Patients	0.08 ± 0.04	14	9.09 ± 4.13	7	50.0	78.6
	Controls	N/A	27	8.48 ± 4.62	N/A	N/A	66.7
Early FU	Patients	2.93 ± 0.81	13	9.78 ± 3.94	6	46.2	76.9
	Controls	N/A	20	8.97 ± 4.03	N/A	N/A	65.0
Late FU	Patients	12.5 ± 2.92	18	10.3 ± 4.00	11	61.1	66.7
	Controls	N/A	26	10.7 ± 3.76	N/A	N/A	61.5

49 unique control subjects were included overall; 30 unique patients were included overall. *, no significant differences in age between patients and controls at each timepoint (all t test p>0.572); **, diagnosis of CMS applied post-operatively; CMS, cerebellar mutism syndrome; FU, follow up.

Fibre tracking

Automated fibre segmentation successfully identified the cerebellar peduncles in the majority of participants; an example patient is shown in Figure 1. Some fibres were excluded after visual inspection. While different fibres were excluded at different timepoints, a larger proportion was discarded at peri-operative timepoints owing to distorted brain anatomy due to the tumour mass effect or resection cavity. Table 2 provides a detailed breakdown of fibres included at each timepoint.

Along-tract profiles of cerebellar peduncles

The results of both analysis approaches (along-tract profiles with permutation-based multiple comparison corrected significance tests; and mixed ANOVAs, *post-hoc* tests, and z-score plots) are described in tandem with reference to each tract, below. Mixed ANOVA results are reported in full in Supplementary Table 1.

Superior cerebellar peduncles

The left SCP showed the greatest effect sizes in group comparisons of along tract FA profiles. Pre-operatively, the difference in distal left SCP FA between controls

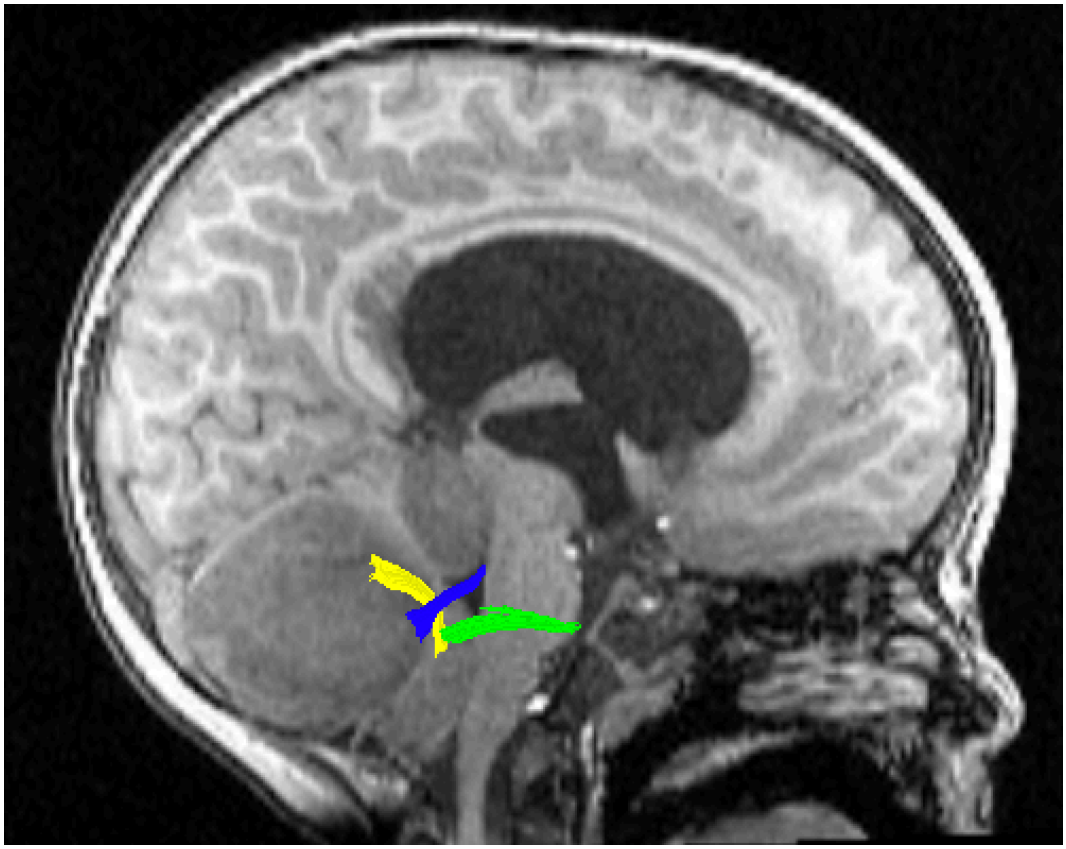

Figure 1 | Example of AFQ-segmented tracts in a representative subject with medulloblastoma. Blue; superior cerebellar peduncle; yellow, inferior cerebellar peduncle; green, middle cerebellar peduncle.

and patients was statistically significant (Figure 2A/i), but patients could not be distinguished based on their CMS status (a classification which was applied retrospectively, following tumour resection). Immediately following surgery, along-tract profiles showed that left SCP FA increased in patients without CMS, but remained lower, especially distally, in those with CMS (Figure 2A/ii). At early follow-up scanning, there were significant differences in proximal left SCP FA between controls, patients with CMS and patients without; differences at the distal SCP did not reach the cluster size for statistical significance (Figure 2A/iii). At the late follow-up timepoint, there were statistically significant group differences at almost all nodes along the tract (Figure 2A/iv).

At the pre-operative timepoint (Figure 3A/i), mixed ANOVA analysis in tract segments of the left SCP showed no significant main effect of CMS status alone ($p=0.957$). The interaction between tract segment and CMS status was not statistically significant ($p=0.798$). There was a significant main effect of tract

Table 2 | Breakdown of fibre groups included by timepoint.

		Right ICP	Left ICP	MCP	Right SCP	Left SCP	Sum / mean (%)
Pre-op	No. with dMRI available (*N*)	17	17	17	17	17	
	Excluded due to indeterminate CMS status	4	4	4	4	4	
	AFQ unable to segment	1	2	0	2	2	7
	AFQ produced erroneous segmentations	7	2	8	2	1	20
	Final *n* (%)	5	9	5	9	10	
	n/N, %	29.4	52.9	29.4	52.9	58.8	44.7
	CMS-	3	3	2	6	7	
	CMS+	2	6	3	3	3	
Post-op	No. with dMRI available (*N*)	17	17	17	17	17	
	Excluded due to indeterminate CMS status	3	3	3	3	3	
	AFQ unable to segment	0	1	1	2	1	5
	AFQ produced erroneous segmentations	0	0	4	4	0	8
	Final *n* (%)	14	13	9	8	13	
	n/N, %	82.4	76.5	52.9	47.1	76.5	67.1
	CMS-	7	7	6	4	6	
	CMS+	7	6	3	4	7	
Early FU	No. with dMRI available (*N*)	15	15	15	15	15	
	Excluded due to indeterminate CMS status	2	2	2	2	2	
	AFQ unable to segment	0	0	0	1	1	2
	AFQ produced erroneous segmentations	0	0	3	1	0	4
	Final *n* (%)	13	13	10	11	12	
	n/N, %	86.7	86.7	66.7	73.3	80.0	78.7
	CMS-	7	7	6	7	7	
	CMS+	6	6	4	4	5	
Late FU	No. with dMRI available (*N*)	21	21	21	21	21	
	Excluded due to indeterminate CMS status	3	3	3	3	3	
	AFQ unable to segment	1	2	1	1	1	6
	AFQ produced erroneous segmentations	3	1	0	2	0	7
	Final *n* (%)	14	15	17	15	17	
	n/N, %	66.7	71.4	81.0	71.4	81.0	74.3
	CMS-	7	7	7	7	7	
	CMS+	7	8	10	8	10	
Mean n/N per tract (%)		66.3	71.9	57.5	61.2	74.1	

segment on z-score (p=0.005), with significant differences also seen on *post-hoc* testing between distal vs proximal two thirds of the left SCP (p=0.014 for both).

At the post-operative timepoint (Figure 3A/ii), mixed ANOVA analysis in the left SCP showed a persistent main effect of tract segment (p<0.001), underpinned by a significant difference between proximal and distal SCP (p=0.026). There were no significant effects of CMS (p=0.341) or its interaction with tract segment (p=0.102). *Post-hoc* testing showed that while distal left SCP FA was lower in the CMS group, this did not reach a level of statistical significance (p=0.1).

At early follow-up scanning (Figure 3A/iii), mixed ANOVA analysis in the left SCP showed a significant interaction between CMS status and tract segment (p=0.006). *Post-hoc* testing revealed that this was due to statistically significant differences at the distal SCP (p=0.042). There were no significant main effects of CMS alone (p=0.209) or tract segment (p=0.163) at this timepoint.

At late follow-up scanning (Figure 3A/iv) , mixed ANOVA analysis in the left SCP showed a persistent significant interaction between tract segment and CMS (p=0.006), which was again statistically significant at the distal left SCP (p=0.038). There was a significant main effect of tract segment (p=0.028), but no significant pairwise differences on *post-hoc* testing. There was no significant effect of CMS alone (p=0.162).

Along-tract FA profiles of the right SCP showed similar – although slightly weaker – associations to its contralateral counterpart. Pre-operatively, there was a statistically significant difference between groups towards the distal right SCP (Figure 2B/i). Post-operatively and at early follow-up scanning, cluster sizes of group differences in along-tract FA results did not reach the threshold of statistical significance (Figures 2B/ii and iii). At late follow-up scanning, there were statistically significant group differences at almost all nodes along the tract (Figure 2B/iv).

Mixed ANOVA analysis along the right SCP did not demonstrate any statistically significant interactions of CMS and tract segment at any timepoint (Figure 3B). There were also no significant effects of CMS status or tract segment alone, at any timepoint, in the right SCP.

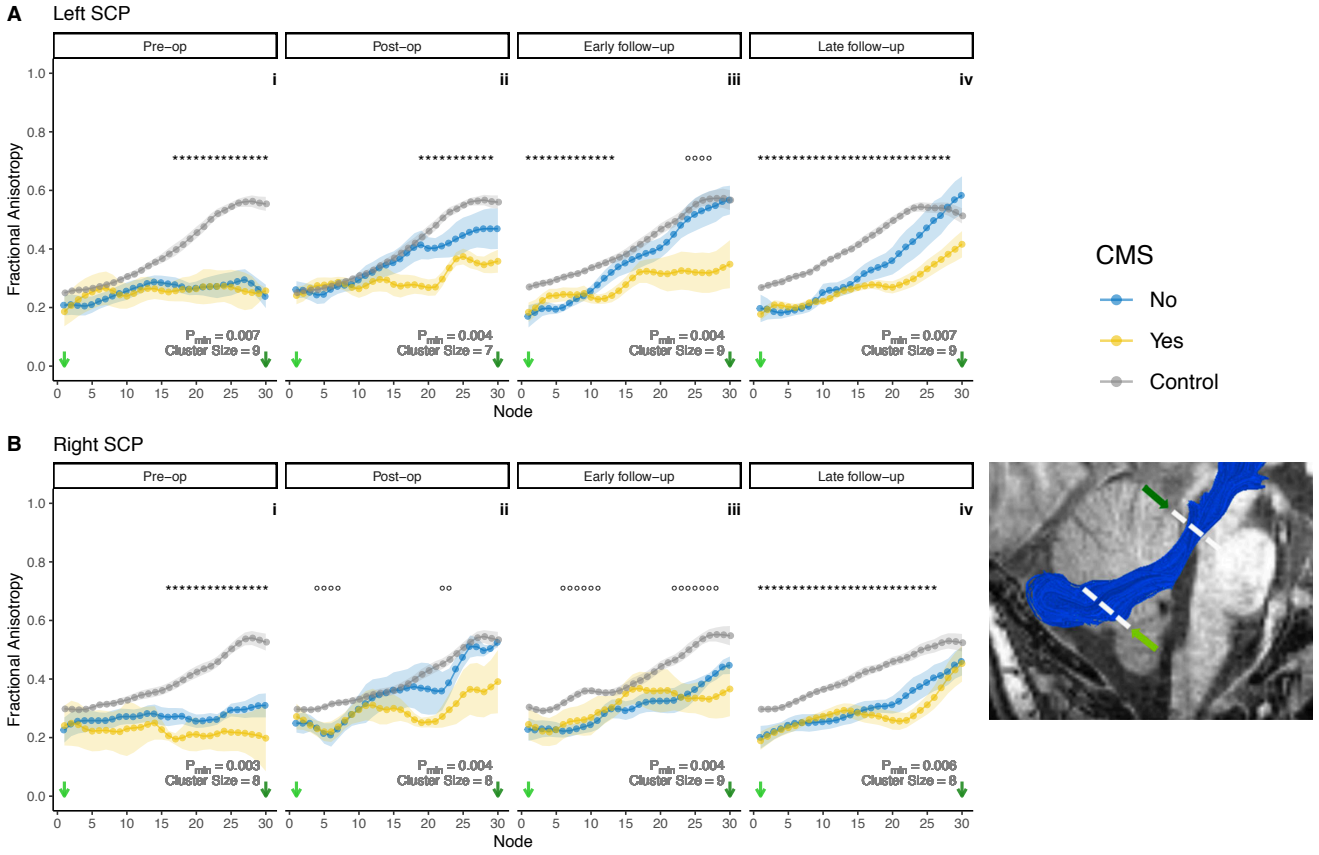

Figure 2 | Longitudinal along-tract profilometry results for the superior cerebellar peduncles (SCP) in patients and controls across four timepoints, pre-op (i) to late follow-up (iv). **A**, left SCP; **B**, right SCP. Points indicate group mean at each node; ribbon indicates standard error of the mean per group. ° indicates by-node ANOVA p-value (p_{var}) lower than the p_{min} calculated by non-parametric permutation method, at that individual node; * indicates $p_{var} < p_{min}$ at more than λ adjacent nodes, where λ is the cluster size for a given tract and timepoint. Cluster size and p_{min} indicated for each tract and timepoint. Bottom right inset shows a representative example of a segmented SCP in a healthy control, from Bruckert *et al.*[24]. Coloured green arrows on inset corresponds to node number on plots.

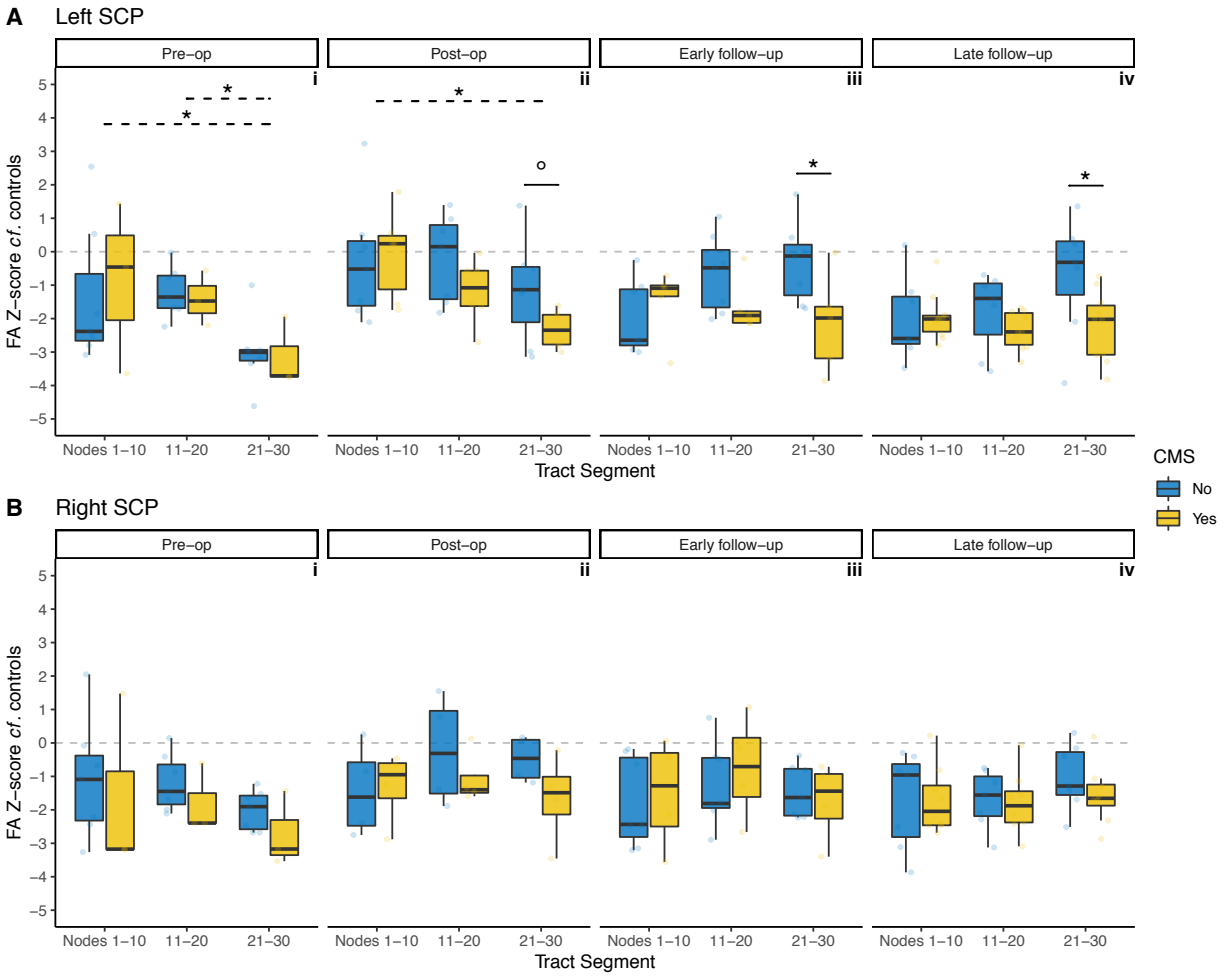

Figure 3 | Z-score of FA for patients with CMS (yellow) and without (blue), compared to controls, within tract segments (proximal / middle / distal thirds) of the superior cerebellar peduncles (SCP). **A**, left SCP; **B**, right SCP. Grey dotted line indicates z = 0. False discovery rate adjusted p values: °, p<0.1; *, p<0.05. Solid lines indicate *post-hoc* pairwise significance tests between CMS groups within tract segments; dotted lines indicate *post-hoc* pairwise significance tests between tract segments.

Inferior Cerebellar Peduncles

There were no statistically significant clusters of group differences in along-tract FA profiles for the left ICP (Figure 4A).

Mixed ANOVA analysis along the left ICP (Figure 5A) did not reveal any statistically significant effects of CMS or its interaction with tract segment, at any timepoint. This analysis did reveal statistically significant effects of tract segment in determining FA z-score for the left ICP at all timepoints apart from pre-operatively ($p<0.001$ post-operative; $p=0.039$ early follow-up; $p=0.033$ late follow-up). *Post-hoc* pairwise comparison tests were reached statistical significance at the post-operative timepoint between the first and second ($p=0.003$), and first and third ($p=0.002$) segments of the tract (Figure 5A/ii).

Pre-operative along-tract FA profiles of the right ICP showed a significant cluster of group differences in the proximal tract (Figure 4B/i). Post-operatively and at early follow-up scanning, cluster sizes of group differences in along-tract FA results did not reach the threshold of statistical significance (Figures 4B/ii and iii). At late follow-up scanning, the same cluster observed at the pre-operative timepoint was again apparent (Figure 4B/iv).

Mixed ANOVA analysis in the right ICP at the pre-operative timepoint (Figure 5B/i) did not reveal statistically significant main effects of tract segment ($p=0.059$) or CMS alone ($p=0.314$). There was also no significant main effect for interaction of tract segment with CMS ($p=0.254$). Although *post-hoc* pairwise comparison testing at the proximal right ICP showed markedly lower z-scores in children with CMS than in those without, this did not reach a level of statistical significance ($p=0.053$).

Post-operatively, mixed ANOVA analysis in the right ICP (Figure 5B/ii) showed a significant main effect of tract segment ($p=0.003$), although pairwise comparisons of tract segment at this timepoint did not survive multiple comparison correction. There was no significant main effect of CMS status ($p=0.310$) or its interaction with tract segment ($p=0.934$).

At early follow-up, mixed ANOVA analysis in the right ICP (Figure 5B/iii) showed a significant main effect for tract segment ($p=0.006$) and its interaction with CMS ($p=0.019$). *Post-hoc* pairwise testing at the proximal right ICP showed lower z-scores in children with CMS than in those without, but this did not reach a level of

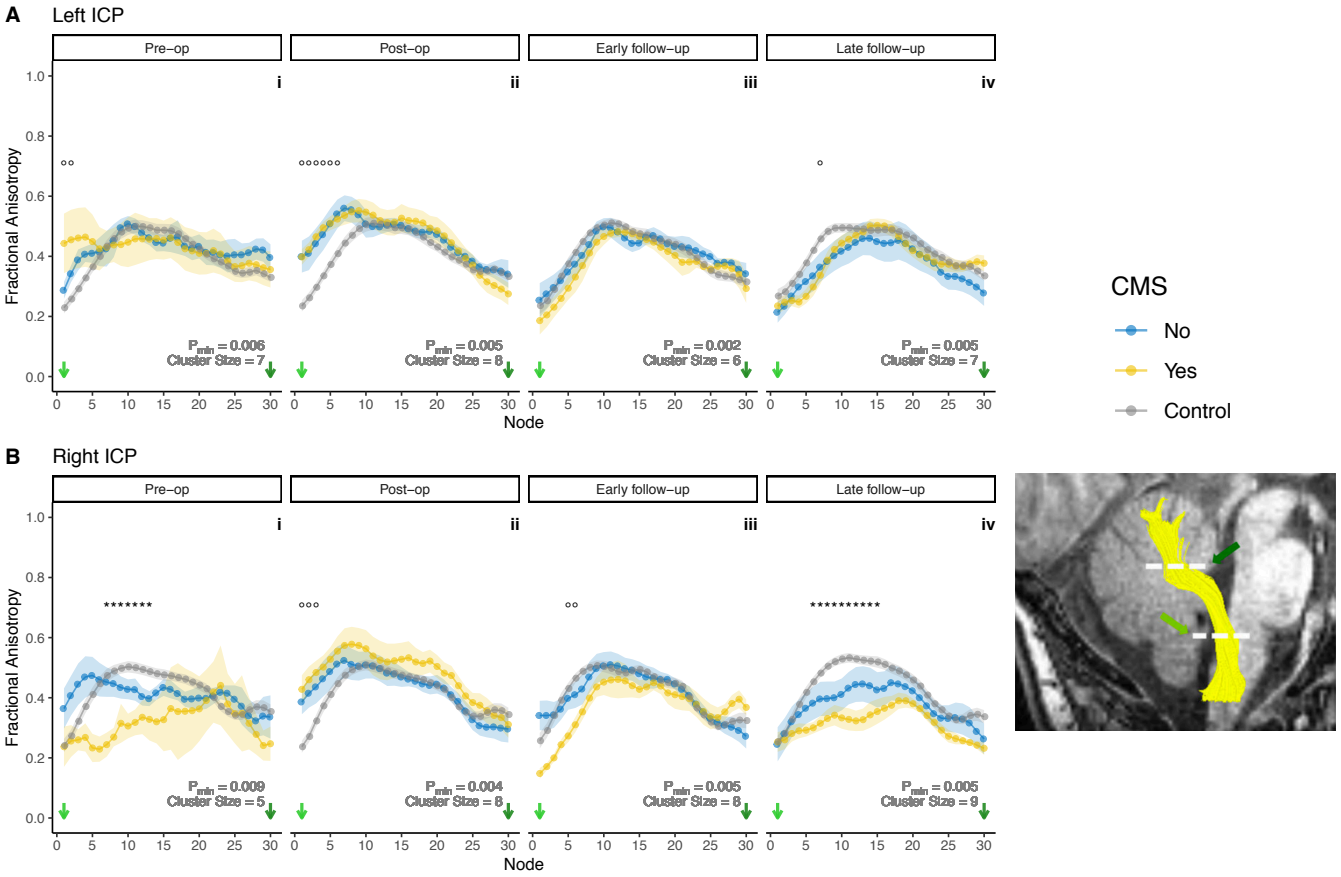

Figure 4 | Longitudinal along-tract profilometry results for the inferior cerebellar peduncles (ICP) in patients and controls across four timepoints, pre-op (i) to late follow-up (iv). **A**, left ICP; **B**, right ICP. Points indicate group mean at each node; ribbon indicates standard error of the mean per group. ° indicates by-node ANOVA p-value (p_{var}) lower than the p_{min} calculated by non-parametric permutation method, at that individual node; * indicates $p_{var} < p_{min}$ at more than λ adjacent nodes, where λ is the cluster size for a given tract and timepoint. Cluster size and p_{min} indicated for each tract and timepoint. Bottom right inset shows a representative example of a segmented ICP in a healthy control, from Bruckert *et al.*[24]. Coloured green arrows on inset corresponds to node number on plots.

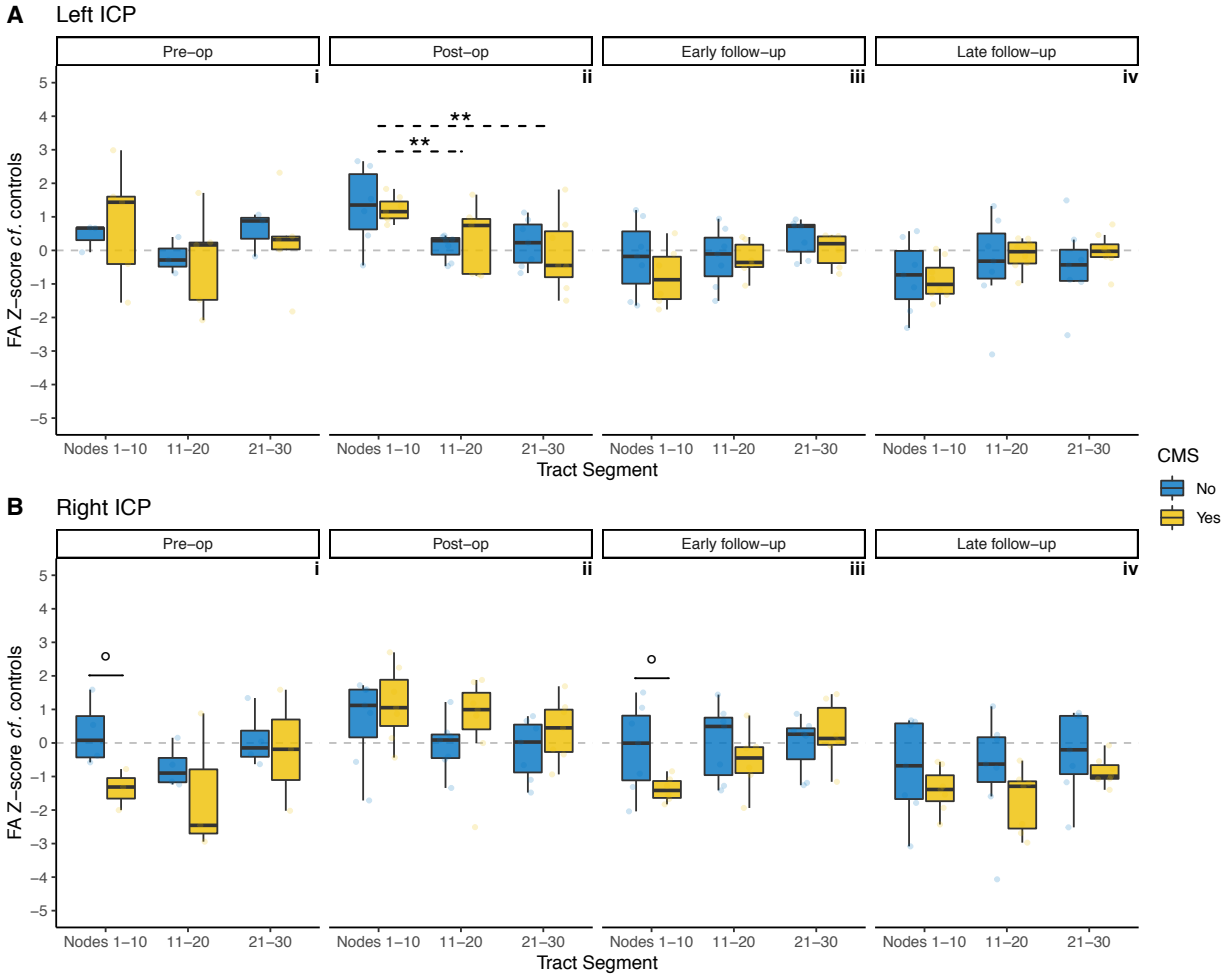

Figure 5 | Z-score of FA for patients with CMS (yellow) and without (blue), compared to controls, within tract segments (proximal / middle / distal thirds) of the inferior cerebellar peduncles (ICP). **A**, left ICP; **B**, right ICP. Grey dotted line indicates z = 0. False discovery rate adjusted p values: °, p<0.1; *, p<0.05. Solid lines indicate *post-hoc* pairwise significance tests between CMS groups within tract segments; dotted lines indicate *post-hoc* pairwise significance tests between tract segments.

statistical significance (p=0.051). CMS alone had a non-significant main effect at this timepoint (p=0.332).

At late follow-up scanning, mixed ANOVA analysis along the right ICP (Figure 5B/iv) did not show significant main effects of CMS (p=0.202), tract segment (p=0.054), or their interactions (p=0.771).

Middle Cerebellar Peduncles

The MCP tract profiles did not show any statistically significant differences between groups at any individual node, and therefore no significant clusters of group differences. There were no significant main effects of CMS, tract segment or their interactions at any timepoint. Results for the MCP are shown in Figure 6.

Discussion

In this retrospective cohort study of children undergoing resective surgery of posterior fossa medulloblastoma, automated along-tract profilometry was used to investigate longitudinal spatiotemporal changes in FA in the cerebellar peduncles. It is shown that reductions in post-operative FA in children with CMS are highly specific to the SCPs; that these changes persist up to one year after surgery, and that the effects are particularly localised to the distal left SCP. Detailed spatial localisation of cerebellar DTI changes in CMS afforded by the automated tractography technique, multiple timepoint sampling and careful matching of patients to controls, are particular strengths of this work.

dMRI metrics in CMS

The first report of altered DTI metrics in children with CMS[11] studied a group of 26 medulloblastomas, half of whom developed CMS post-operatively. FA was found to be significantly reduced in bilateral SCPs, as well as in supratentorial white matter subtending the right angular gyrus, the left superior frontal gyrus, and also in the columns of the fornix[11].

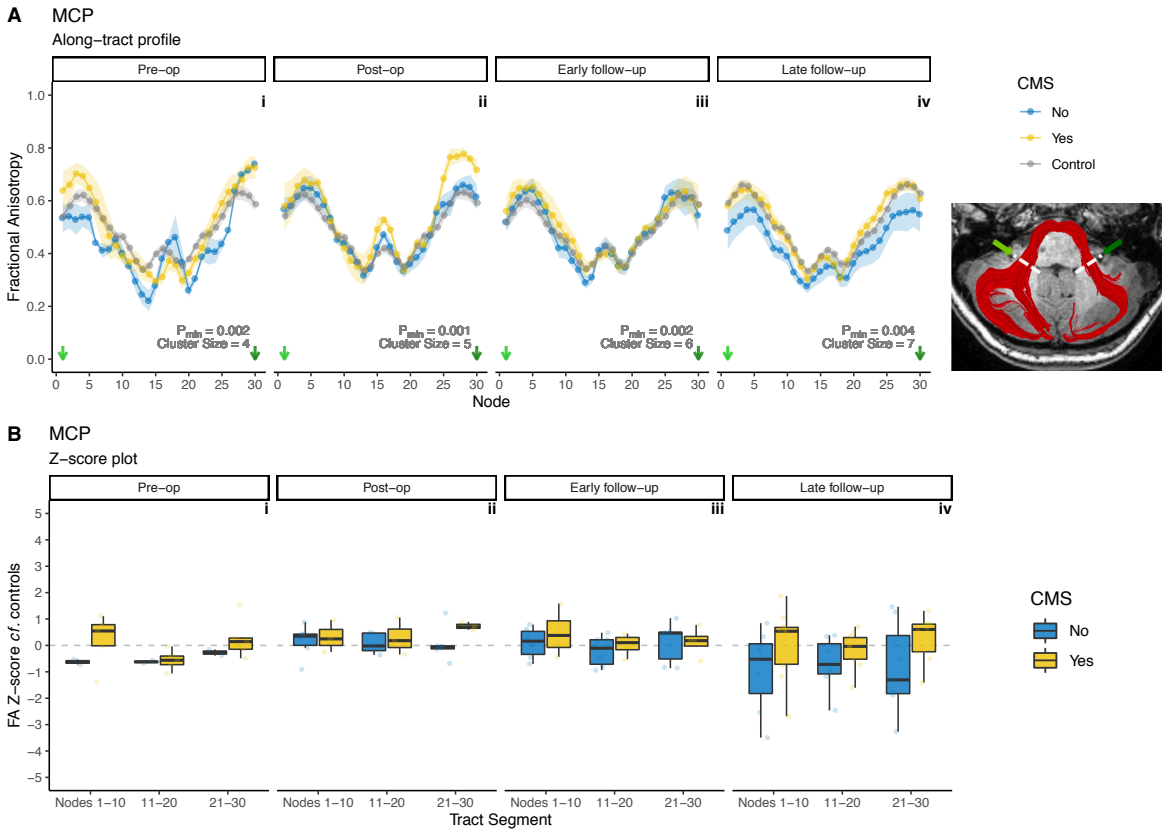

Figure 6 | A, Along-tract profiles of the middle cerebellar peduncle (MCP) in patients and controls, across four timepoints, pre-operative (i) to late follow-up (iv). There were no statistically significant differences between groups at any individual node. Inset shows a representative example of a segmented MCP in a healthy control, from Bruckert *et al.*[24]. Coloured green arrows on inset corresponds to node number on plots. **B**, Z-score of FA for patients with CMS (yellow) and without (blue), compared to controls, within tract segments (proximal / middle / distal thirds) of the middle cerebellar peduncles (MCP). Grey dotted line indicates z = 0. There were no statistically significant differences with respect to CMS status.

This early finding of FA changes in the SCPs of children with CMS paved the way for further applications of dMRI in this patient population, with a variety of metrics being reported. Law *et al.*, 2012 showed significant group differences in mean, axial and radial diffusivity (but not FA) in right cerebellar white matter based on deterministic tractography in a group of 51 children with heterogeneous posterior fossa tumours (17 of whom developed CMS), and 28 healthy controls[18]. Qualitative assessment of direction-encoded colour FA maps[35] and intra-operative diffusion-weighted MRI[36] showed SCP damage in children with CMS. Tract volumes of fronto-cerebellar fibre tracts have also been shown to be diminished in children with CMS[17].

A distinctive feature of the present study is the investigation of cerebellar white matter tracts in cerebellar mutism over time from pre-surgical to 1-year post-operative. The aforementioned studies all concern the application of dMRI at a single, post-operative timepoint. Given the striking temporal course of CMS semiology – beginning days after tumour resection and usually receding after a few months – longitudinal MRI studies are apt in this clinical population. A longitudinal study at three timepoints (pre-op, post-op and 1 year follow-up) showed statistically significant post-operative reductions in FA of both SCPs which persisted up to 1 year[13]. A similarly designed study showed post-operative reductions in FA in the left SCP only, and these changes were persistent in patients with ongoing ataxia at delayed follow-up imaging, but not in those with ongoing symptoms of mutism[14].

The results of presented in this essay confirm no statistically significant differences in pre-operative FA of any cerebellar peduncle with respect to CMS status. Neither of the latter two studies demonstrated pre-operative changes in FA at the SCP in patients who went on to develop CMS[13,14]. These reports indicate FA is unsuitable as a pre-operative marker of CMS risk, as is also the case for T2-weighted signal change[37].

Spatial sensitivity of along-tract profilometry in CMS

The present study used along-tract profilometry, an offshoot of dMRI post-processing which enables the sampling of dMRI metrics along the long axis of a tract, rather than within regions of interest on a voxel-wise basis. Several implementations of this processing method exist[20,22], and here we report a novel application of one of the earliest such toolboxes, AFQ[21]. Initially devised as a means of segmenting major supratentorial white matter tracts, a later extension to the toolbox added cerebellar peduncle segmentation[23,24], and this application has been

used to study reading ability in healthy children[38], locomotor adaptation in healthy adults[39] and cerebellar microstructure in preterm-born adolescents[25].

A major advantage of the AFQ pipeline in this instance is its ability to identify the location-dependent changes in FA at the SCP. Studies reporting DTI metrics in the SCP[11,13–15] do not describe spatial localisation of changes within the tract. Inspection of Figure 2 of Morris *et al.*'s work[11] shows that the FA changes were seen across the entirety of both SCPs, with some retrograde extension into the cerebellar white matter. SCP ROIs in Vedantam *et al.*[14] appear to have been placed on three axial slices, and FA results averaged across these. McEvoy *et al.*[13] used ROIs from a co-registered DTI atlas[40], with FA averaging within the ROI. The present results demonstrate that changes in FA are focused on the distal SCP as it approaches the midbrain rather than its more proximal portion as it exits the cerebellar parenchyma. Furthermore, assessing these changes over four timepoints (including pre-operatively), with at least 13 patients at each being compared to a robust number of age- and sex-matched controls, makes the present study a richly sampled dataset in comparison to other series.

Complementary analysis techniques were used to assess differences in along-tract FA. First, differences in mean FA of each group (controls, CMS and non-CMS) were compared at each of thirty nodes along the segmented tracts, using one-way ANOVA. Due to the high degree of auto-correlation between adjacent nodes, a non-parametric permutation based method was used to generate a p value (p_{min}) adjusted for multiple comparisons, as well as a minimum cluster size for truly significant group differences. Figures 2 and 4 show that significant clusters were concentrated mainly in the SCPs (more so on the left), with smaller clusters in the right ICP. There were no significant group differences in along-tract FA for the MCP or left ICP.

Another innovation of the present study was converting patients' FA values to z-scores based on the controls' summary statistics of FA at each node. This method allowed a comparison of the magnitude of difference in FA between the patient cohort and the control children, as well as an assessment of differences within the patient cohort with respect to CMS status. The z-score of distal SCP FA in children with CMS was -2 (in other words, around 2 standard deviations lower than the control mean); whereas children without CMS had z-scores in this location much closer to 0 (i.e. similar to mean FA of controls at those nodes). Crucially, mixed ANOVA showed a significant main effect of interaction between CMS and tract

segment at these two timepoints (p=0.006 for both), driven by statistically significant differences at the distal SCP. This finding mirrors the robust significant cluster in Figure 3D; there is no significant cluster at the distal SCP in Figure 3C due to the close similarity between control and non-CMS groups in this plot.

The findings presented in this essay suggest that changes in cerebellar white matter in CMS are highly localized at the more rostral portion of the SCP – in other words, the part of the SCP which forms the lateral walls of the fourth ventricle. If damage to the SCP in CMS is putatively caused at the time of surgery, neurosurgeons performing tumour resections in this location will wisely treat this area with extreme caution, particularly as fibres to the supplementary motor area, with its key involvement in speech generation, are thought to reside in the medial – and therefore more likely to suffer surgical damage – edge of the SCP[9]. Although mixed ANOVA found these spatial differences to be significant at follow-up timepoints only, along-tract analyses also indicated evidence of group differences in the distal SCP at post-operative imaging, making it possible that surgical damage contributes to acute, as well as chronic, changes in FA in the distal SCP.

Fundamentally, reduced FA in this white matter bundle reflects a greater degree of directional incoherence – or, in a biophysical sense, less uniformly arrayed axons. However, FA encodes both microscopic diffusion processes (i.e. related to the density of fibres) as well as orientational information. More advanced models of the diffusion signal, such as the spherical mean technique[41], are able to distinguish between these two components and can more precisely estimate changes in orientational tissue properties. Combining spherical mean technique modelling with AFQ profilometry could yield further insights into the fine-grained microstructural properties of cerebellar peduncles in children with CMS.

Limitations

This study effectively builds on previous work and is the most comprehensive longitudinal analysis of CMS patients using DTI to date. A limitation is the modest sample size for some groups and timepoints (e.g. pre-operatively, the right ICP and MCP analysis only contained 5 patients). The numbers of viable tracts included in the analyses were unavoidably reduced at the stage of visual inspection of AFQ fibre segmentations. This problem was most commonly seen at the peri-operative timepoints, appreciably due to anatomical distortion from tumours in pre-operative, and resection cavities in post-operative scans. By the early follow-up timepoint, however, 78.7% of fibre groups segmented by AFQ were found to be viable. Across

all timepoints, AFQ segmentation of the left SCP was the most robust, deemed anatomically accurate in 52/70 (74.1%) cases.

The lack of a clear, objective determination of CMS status is a perennial issue in studies reporting neuroimaging correlates of the syndrome and this criticism applies to this study. The diagnoses of CMS were applied based on retrospective review of case notes. In cases where no clear contemporaneous description of mutism was annotated, these were classified as having indeterminate CMS status and excluded from the imaging analyses. It should be noted that the incidence of CMS seen in this study (13/30, 43.3%) is not representative of CMS incidence for posterior fossa tumours more generally, as this was an enriched sample of mostly midline posterior fossa tumours, which are known to have a higher risk of developing CMS[42].

One outstanding issue which this study does not resolve is the element of laterality in SCP abnormalities in children with CMS. Reports in healthy children[9] and adults[43] indicate no differences in FA or other diffusion MRI metrics between left and right DRTC tracts. However, many of the aforementioned studies have drawn different conclusions as to the required laterality of SCP damage in CMS; be it left[14] – which our results are in agreement with – right[18], or bilateral[11,13,35,36,44]. This may be due in part to the small sample sizes seen in many of these reports, and collaborative multi-centre approaches to tackle this problem may provide more definitive answers.

Conclusions

A novel application of an automated tool to extract diffusion MRI metrics along the length of the cerebellar peduncles is described in a longitudinal retrospective cohort of paediatric medulloblastoma with and without cerebellar mutism syndrome. Changes in FA in the cerebellar peduncles are described in a heretofore unprecedented level of spatiotemporal detail. There were no pre-surgical changes in FA which with respect to subsequent CMS status. Children with post-operative CMS showed focal changes in the distal regions of the left SCP, and these changes persisted up to a year post-operatively. These findings have direct clinical implications for neurosurgeons performing resection of midline paediatric posterior fossa tumours.

References

1 Toescu SM, Samarth G, Horsfall HL, Issitt R, Margetts B, Phipps K *et al.* Fourth ventricle tumors in children: complications and influence of surgical approach. *J Neurosurg Pediatr* 2020. doi:10.3171/2020.6.PEDS2089.

2 Gudrunardottir T, Sehested A, Juhler M, Grill J, Schmiegelow K. Cerebellar mutism: definitions, classification and grading of symptoms. *Child's Nerv Syst* 2011; **27**: 1361–1363.

3 Wibroe M, Ingersgaard MV, Larsen HB, Juhler M, Piil K. Living with the cerebellar mutism syndrome: long-term challenges of the diagnosis. *Acta Neurochir (Wien)* 2020. doi:10.1007/s00701-020-04479-3.

4 De Smet HJ, Baillieux H, Wackenier P, De Praeter M, Engelborghs S, Paquier PF *et al.* Long-term cognitive deficits following posterior fossa tumor resection: a neuropsychological and functional neuroimaging follow-up study. *Neuropsychology* 2009; **23**: 694–704.

5 Cámara S, Fournier MC, Cordero P, Melero J, Robles F, Esteso B *et al.* Neuropsychological Profile in Children with Posterior Fossa Tumors with or Without Postoperative Cerebellar Mutism Syndrome (CMS). *Cerebellum* 2020; **19**: 78–88.

6 Patay Z. Postoperative posterior fossa syndrome: unraveling the etiology and underlying pathophysiology by using magnetic resonance imaging. *Childs Nerv Syst* 2015; **31**: 1853–8.

7 Ji Q, Edwards A, Glass JO, Brinkman TM, Patay Z, Reddick WE. Measurement of Projections Between Dentate Nucleus and Contralateral Frontal Cortex in Human Brain Via Diffusion Tensor Tractography. *The Cerebellum* 2019; : 1–9.

8 Palesi F, Tournier JD, Calamante F, Muhlert N, Castellazzi G, Chard D *et al.* Contralateral cerebello-thalamo-cortical pathways with prominent involvement of associative areas in humans in vivo. *Brain Struct Funct* 2015; **220**: 3369–3384.

9 Toescu SM, Hales PW, Kaden E, Lacerda LM, Aquilina K, Clark CA. Tractographic and Microstructural Analysis of the Dentato-Rubro-Thalamo-Cortical Tracts in Children Using Diffusion MRI. *Cereb Cortex* 2020. doi:10.1093/cercor/bhaa377.

10 Avula S, Spiteri M, Kumar R, Lewis E, Harave S, Windridge D *et al.* Post-operative pediatric cerebellar mutism syndrome and its association with hypertrophic olivary degeneration. *Quant Imaging Med Surg* 2016; **6**: 535–544.

11 Morris EB, Phillips NS, Laningham FH, Patay Z, Gajjar A, Wallace D *et al.* Proximal dentatothalamocortical tract involvement in posterior fossa syndrome. *Brain* 2009; **132**: 3087–3095.

12 Perreault S, Lober RM, Cheshier S, Partap S, Edwards MS, Yeom KW. Time-dependent structural changes of the dentatothalamic pathway in children treated for posterior fossa tumor. *Am J Neuroradiol* 2014; **35**: 803–807.

13 McEvoy SD, Lee A, Poliakov A, Friedman S, Shaw D, Browd SR *et al.* Longitudinal cerebellar diffusion tensor imaging changes in posterior fossa syndrome. *NeuroImage Clin* 2016; **12**: 582–590.

14 Vedantam A, Stormes KM, Gadgil N, Kralik SF, Aldave G, Lam SK. Association

between postoperative DTI metrics and neurological deficits after posterior fossa tumor resection in children. 2019; : 1–7.

15 Van Baarsen K, Kleinnijenhuis M, Konert T, Van Cappellen Van Walsum AM, Grotenhuis A. Tractography demonstrates dentate-rubro-thalamic tract disruption in an adult with cerebellar mutism. *Cerebellum* 2013; **12**: 617–622.

16 Smith SM, Jenkinson M, Johansen-Berg H, Rueckert D, Nichols TE, Mackay CE *et al.* Tract-based spatial statistics: Voxelwise analysis of multi-subject diffusion data. *Neuroimage* 2006; **31**: 1487–1505.

17 Soelva V, Hernáiz Driever P, Abbushi A, Rueckriegel S, Bruhn H, Eisner W *et al.* Fronto-cerebellar fiber tractography in pediatric patients following posterior fossa tumor surgery. *Childs Nerv Syst* 2013; **29**: 597–607.

18 Law N, Greenberg M, Bouffet E, Taylor MD, Laughlin S, Strother D *et al.* Clinical and neuroanatomical predictors of cerebellar mutism syndrome. *Neuro Oncol* 2012; **14**: 1294–303.

19 Smith RE, Raffelt D, Tournier J, Connelly A. Quantitative streamlines tractography : methods and inter-subject normalisation. *bioRxiv* 2020; : 1–27.

20 Dayan M, Monohan E, Pandya S, Kuceyeski A, Nguyen TD, Raj A *et al.* Profilometry: A new statistical framework for the characterization of white matter pathways, with application to multiple sclerosis. *Hum Brain Mapp* 2016; **37**: 989–1004.

21 Yeatman JD, Dougherty RF, Myall NJ, Wandell BA, Feldman HM. Tract Profiles of White Matter Properties: Automating Fiber-Tract Quantification. *PLoS One* 2012; **7**. doi:10.1371/journal.pone.0049790.

22 Chandio BQ, Risacher SL, Pestilli F, Bullock D, Yeh FC, Koudoro S *et al.* Bundle analytics, a computational framework for investigating the shapes and profiles of brain pathways across populations. *Sci Rep* 2020; **10**: 1–18.

23 Leitner Y, Travis KE, Ben-Shachar M, Yeom KW, Feldman HM. Tract Profiles of the Cerebellar White Matter Pathways in Children and Adolescents. *The Cerebellum* 2015; **14**: 613–623.

24 Bruckert L, Shpanskaya K, McKenna ES, Borchers LR, Yablonski M, Blecher T *et al.* Age-Dependent White Matter Characteristics of the Cerebellar Peduncles from Infancy Through Adolescence. *The Cerebellum* 2019; : 1–16.

25 Travis KE, Leitner Y, Ben-Shachar M, Yeom KW, Feldman HM. Case Series. *J Child Neurol* 2016; **31**: 321–327.

26 Li X, Morgan PS, Ashburner J, Smith J, Rorden C. The first step for neuroimaging data analysis: DICOM to NIfTI conversion. *J Neurosci Methods* 2016; **264**: 47–56.

27 Basser PJ, Pajevic S, Pierpaoli C, Duda J, Aldroubi A. In vivo fiber tractography using DT-MRI data. *Magn Reson Med* 2000; **44**: 625–32.

28 Conturo TE, Lori NF, Cull TS, Akbudak E, Snyder AZ, Shimony JS *et al.* Tracking neuronal fiber pathways in the living human brain. *Proc Natl Acad Sci U S A* 1999; **96**: 10422–7.

29 Mori S, Crain BJ, Chacko VP, van Zijl PC. Three-dimensional tracking of axonal projections in the brain by magnetic resonance imaging. *Ann Neurol* 1999; **45**: 265–9.

30 Wickham H. ggplot2: Elegant Graphics for Data Analysis. 2009.

31 Kassambara A. rstatix: Pipe-Friendly Framework for Basic Statistical Tests. 2020.

32 Kassambara A. ggpubr: 'ggplot2' Based Publication Ready Plots. 2019.

33 Nichols TE, Holmes AP. Nonparametric Permutation Tests For Functional Neuroimaging: A Primer with Examples. 2001.

34 Benjamini Y, Hochberg Y. Controlling the False Discovery Rate: A Practical and Powerful Approach to Multiple Testing. J. R. Stat. Soc. Ser. B. 1995; **57**: 289–300.

35 Ojemann JG, Partridge SC, Poliakov A V, Niazi TN, Shaw DW, Ishak GE *et al.* Diffusion tensor imaging of the superior cerebellar peduncle identifies patients with posterior fossa syndrome. *Childs Nerv Syst* 2013; **29**: 2071–7.

36 Avula S, Kumar R, Pizer B, Pettorini B, Abernethy L, Garlick D *et al.* Diffusion abnormalities on intraoperative magnetic resonance imaging as an early predictor for the risk of posterior fossa syndrome. *Neuro Oncol* 2015; **17**: 614–622.

37 Toescu S, Hettige S, Phipps K, Smith R, Haffenden V, Clark C *et al.* Post-operative paediatric cerebellar mutism syndrome: time to move beyond structural MRI. *Child's Nerv Syst* 2018; **in press**. doi:https://doi.org/10.1007/s00381-018-3867-x.

38 Bruckert L, Travis KE, Mezer AA, Ben-Shachar M, Feldman HM. Associations of Reading Efficiency with White Matter Properties of the Cerebellar Peduncles in Children. *Cerebellum* 2020. doi:10.1007/s12311-020-01162-2.

39 Jossinger S, Mawase F, Ben-Shachar M, Shmuelof L. Locomotor Adaptation Is Associated with Microstructural Properties of the Inferior Cerebellar Peduncle. *Cerebellum* 2020; **19**: 370–382.

40 Oishi K, Faria A, van Zijl PCM, Mori S. MRI Atlas of Human White Matter. 2010.https://www.google.co.uk/books/edition/_/v8MWjTpVUAYC?hl=en&gbpv=0 (accessed 22 Dec2020).

41 Kaden E, Kelm ND, Carson RP, Does MD, Alexander DC. Multi-compartment microscopic diffusion imaging. *Neuroimage* 2016; **139**: 346–359.

42 Grønbæk J, Wibroe M, Toescu S, Grillner P, Mallucci C, Molinari E *et al.* Cerebellar Mutism Syndrome and the surgical risk factors: a prospective multicentre study of 500 patients undergoing tumour surgery in the posterior fossa. In: *International Society for Paediatric Neuro-Oncology*. 2020.

43 Kim Y, Im S, Kim S-H, Park G-Y. Laterality of cerebellar afferent and efferent pathways in a healthy right-handed population: A diffusion tensor imaging study. *J Neurosci Res* 2018. doi:10.1002/jnr.24378.

44 Miller NG, Reddick WE, Kocak M, Glass JO, Löbel U, Morris B *et al.* Cerebellocerebral Diaschisis Is the Likely Mechanism of Postsurgical Posterior Fossa Syndrome in Pediatric Patients with Midline Cerebellar Tumors. *Am J Neuroradiol* 2009; **31**: 288–294.

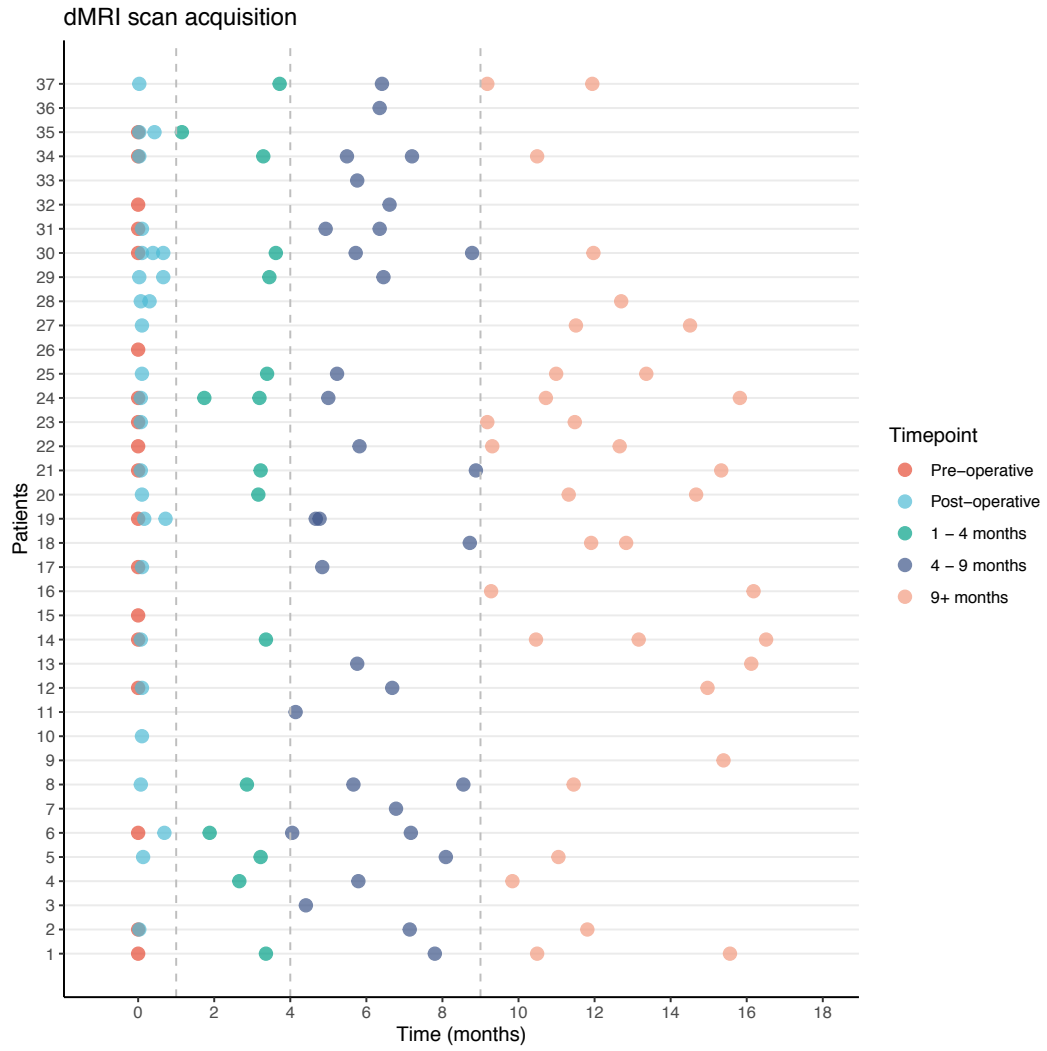

Supplementary Figure 1 | Diffusion MRI scan acquisition for eligible subjects. Scans were grouped into four timepoints: pre-operative, post-operative, early follow-up (1-4 months) and late follow-up (>9 months). Scans acquired between 4 and 9 months post-operatively (purple points) were not included in the analysis.

Supplementary Table 1 | Fractional Anisotropy Z-score mixed ANOVA results.

	Tract segment	Pre-op	Post-op	Early FU	Late FU
Left SCP					
CMS		0.957	0.341	0.209	0.162
Tract segment		**0.005**	**0.000382**	0.163	**0.028**
	1st vs 2nd	0.946	0.389	0.292	0.715
	1st vs 3rd	**0.0137**	**0.0262**	0.292	0.524
	2nd vs 3rd	**0.0137**	0.0979	0.978	0.524
CMS:segment		0.798	0.102	**0.006**	**0.006**
	1st	0.763	0.829	0.477	0.909
	2nd	0.702	0.166	0.145	0.201
	3rd	0.858	0.1	**0.0421**	**0.0381**
Right SCP					
CMS		0.479	0.435	0.848	0.648
Tract segment		**0.045**	0.185	0.05	0.126
	1st vs 2nd	0.842	0.627	0.538	0.936
	1st vs 3rd	0.242	0.627	0.829	0.404
	2nd vs 3rd	0.242	0.627	0.538	0.404
CMS:segment		0.977	0.225	0.338	0.52
	1st	0.718	0.893	0.795	0.999
	2nd	0.358	0.405	0.578	0.816
	3rd	0.221	0.173	0.625	0.297
Left ICP					
CMS		0.985	0.793	0.344	0.617
Tract segment		0.1	**0.00335**	**0.039**	**0.033**
	1st vs 2nd	0.469	**0.00308**	0.451	0.142
	1st vs 3rd	0.646	**0.00177**	0.103	0.142
	2nd vs 3rd	0.489	0.657	0.239	0.949
CMS:segment		0.641	0.449	0.607	0.511
	1st	0.737	0.856	0.348	0.828
	2nd	0.918	0.636	0.9	0.618
	3rd	0.729	0.57	0.233	0.37
Right ICP					
CMS		0.314	0.31	0.332	0.202
Tract segment		0.059	**0.003**	**0.006**	0.054
	1st vs 2nd	0.53	0.203	0.339	0.664
	1st vs 3rd	0.57	0.182	0.128	0.395
	2nd vs 3rd	0.429	0.686	0.391	0.371
CMS:segment		0.254	0.934	**0.019**	0.771
	1st	0.0532	0.461	0.0512	0.309
	2nd	0.497	0.329	0.379	0.218
	3rd	0.771	0.266	0.523	0.3

MCP					
CMS		0.298	0.355	0.488	0.117
Tract segment		0.259	0.516	0.394	0.753
	1st vs 2nd	0.226	0.847	0.595	0.999
	1st vs 3rd	0.698	0.847	0.589	0.999
	2nd vs 3rd	0.222	0.847	0.595	0.999
CMS:segment		0.539	0.47	0.781	0.432
	1st	0.312	0.738	0.427	0.186
	2nd	0.834	0.575	0.503	0.22
	3rd	0.397	0.114	0.985	0.134

Values indicate multiple-comparison corrected *p* values. Cells in bold indicate $p<0.05$.